

Reopening the Higgs Portal for Singlet Scalar Dark Matter

J. A. Casas ^a, D. G. Cerdeño ^{b,a}, J. M. Moreno ^a and J. Quilis ^a

^a Instituto de Física Teórica UAM/CSIC, Universidad Autónoma de Madrid, 28049, Madrid, Spain

^b Institute for Particle Physics Phenomenology, Department of Physics
Durham University, Durham DH1 3LE, United Kingdom

Abstract

A real singlet scalar, connected to the Standard Model sector through a portal with the Higgs boson, is one of the simplest and most popular models for dark matter (DM). However, the experimental advances in direct and indirect DM searches, together with the latest results from the LHC, have ruled out vast areas of the parameter space of this scenario; and are expected to probe it completely within the next years, ruling it out if no signal is found. Motivated by the simplicity of this model, in this article we address a minimal, renormalizable extension that could evade detection, consisting of the addition of an extra real singlet scalar field in the dark sector. We analyze the physical constraints on the model and show that the new annihilation and/or coannihilation channels involving the extra singlet allow to reproduce the correct DM relic abundance while avoiding the bounds from direct and indirect searches for any DM mass above 50 GeV. We also show that, in some interesting regions of the parameter space, the extra particle can be integrated-out, leaving a “clever” effective theory (just involving the DM particle and the Higgs), that essentially reproduces the results.

1 Introduction

The nature of more than 80% of the matter in our Universe is still unknown. Over the past century, substantial evidence has been collected from astrophysical and cosmological observations that supports the existence of a new type of *dark* matter (DM), that does not emit or absorb light, and that cannot be explained by the Standard Model (SM). This window to new physics is currently being thoroughly probed by dedicated direct and indirect DM experiments, as well as by the Large Hadron Collider (LHC), with increasing sensitivities.

Among the many particle physics candidates for DM, the singlet-scalar Higgs portal (SHP) model stands out as one of the most economical and popular scenarios. [1–3]. It simply consists of one extra singlet scalar, S (the DM particle), which is minimally coupled to the SM through interactions with the ordinary Higgs (the only ones allowed at the renormalizable level). The corresponding Lagrangian reads

$$\mathcal{L}_{\text{SHP}} = \mathcal{L}_{\text{SM}} + \frac{1}{2}\partial_\mu S \partial^\mu S - \frac{1}{2}m_0^2 S^2 - \frac{1}{2}\lambda_S |H|^2 S^2 - \frac{1}{4!}\lambda_4 S^4. \quad (1.1)$$

In the previous equation S has been assumed to be a real field, but the modification for the complex case is trivial. Furthermore, a discrete symmetry $S \rightarrow -S$ has been imposed in order to ensure the stability of the DM particle; apart from this, the above renormalizable Lagrangian is completely general. After electroweak (EW) symmetry breaking, the Higgs field acquires a vacuum expectation value, $H^0 = (v + h)/\sqrt{2}$, and new terms appear, including a trilinear coupling between S and the Higgs boson, $(\lambda_S v/2)hS^2$. The phenomenology of this model has been explored in other contexts as well [4–7].

Assuming that the S -particles are in thermal equilibrium in the early universe, the final DM relic density is determined by their primordial annihilation rate into SM-particles. The relevant processes, illustrated in Fig. 1, are usually dominated by the s -channel annihilation through a Higgs boson (leftmost diagram of the figure).

The efficiency of the annihilation depends on just two parameters, $\{m_0, \lambda_S\}$ or, equivalently, $\{m_S, \lambda_S\}$, where $m_S^2 = m_0^2 + \lambda_S v^2/2$ is the physical S -mass after EW breaking. Fig. 2 shows the (black) line in the $\{m_S, \lambda_S\}$ plane along which the relic abundance of S , $\Omega_S h^2$, coincides with the Planck result $\Omega_{CDM} h^2 = 0.1198 \pm 0.003$ at 2σ [8]. The (gray) region below is in principle excluded, as it corresponds to a higher relic density.

The model is subject to a number of experimental and observational constraints, which rule out large regions of the parameter space. These include limits from direct detection experiments [9–21], indirect searches [22–48], as well as collider bounds [49–56]. We illustrate the effects of these limits in Fig. 2. In deriving direct and indirect detection bounds, we are assuming by default (left panel) that the density of S scales up in the same way as its cosmological relic abundance. Thus, we consider a scale factor $\xi \equiv \Omega_S/\Omega_{CDM}$ for direct

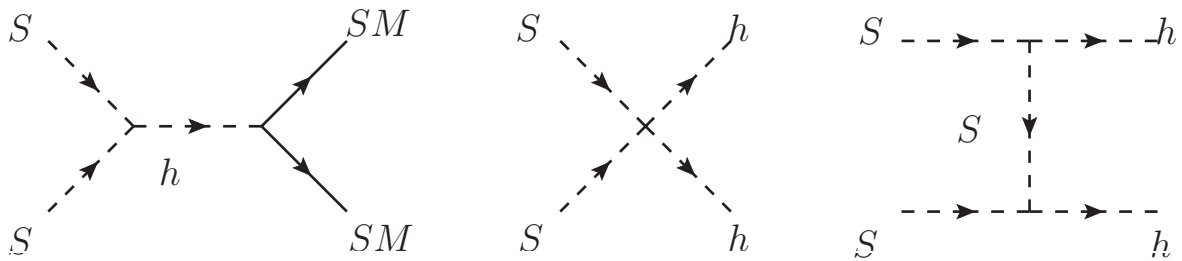


Figure 1: Singlet-scalar Higgs portal scenario (SHP): annihilation processes of the DM candidate, S .

detection and ξ^2 for indirect detection. In the region where $\xi < 1$, S cannot be the only DM component, so contributions from other particles (e.g., axions) are needed. The region where $\xi > 1$ (gray area) is obviously excluded (though perhaps could be rescued if some non-standard cosmology is invoked, see below). For this reason, we have not showed the shadowed regions inside this gray area. It is worth noting that the excluded areas are extremely sensitive to astrophysical uncertainties in the DM halo parameters [57] and nuclear uncertainties in the hadronic matrix elements [47].

Current bounds from direct DM detection, most notably from the new results from LUX [58] and PandaX-II [59], set an upper bound on the DM-nucleon elastic scattering cross section (and hence on the DM coupling to the Higgs). This rules out the red area in Fig. 2. Next-generation experiments, with larger targets and improved sensitivity are going to further explore this parameter space. We indicate in the figure the expected reach of the LZ detector by means of a green dashed line. Similarly, Fermi-LAT data on the continuum gamma-ray flux from dwarf spheroidal galaxies (dSPh) and monochromatic gamma-ray lines from the Galactic Centre set upper bounds on the DM annihilation cross section which also rule out some areas of the parameter space, mainly for DM masses below 100 GeV (light brown and cyan areas respectively). It should be noticed that, as λ_S decreases, the ξ -factor increases, so that the indirect detection rate increases as well. Consequently, the excluded areas from indirect detection extend downwards in the plot. Finally, for masses below ~ 63 GeV, the DM can contribute to the invisible decay of the SM Higgs boson. Current LHC constraints on this quantity set an upper bound on the DM-Higgs coupling [53]. The blue region in Fig. 2 is excluded for this reason.

For comparison, the right panel of Fig. 2 shows the direct and indirect detection constraints when the local DM density is assumed to take the canonical value, $\rho_0 = 0.3 \text{ GeV cm}^{-3}$, regardless of the computed thermal relic abundance; in other words, we have set $\xi = 1$. This would apply if non-thermal effects modified the final relic abundance, reconciling it with the

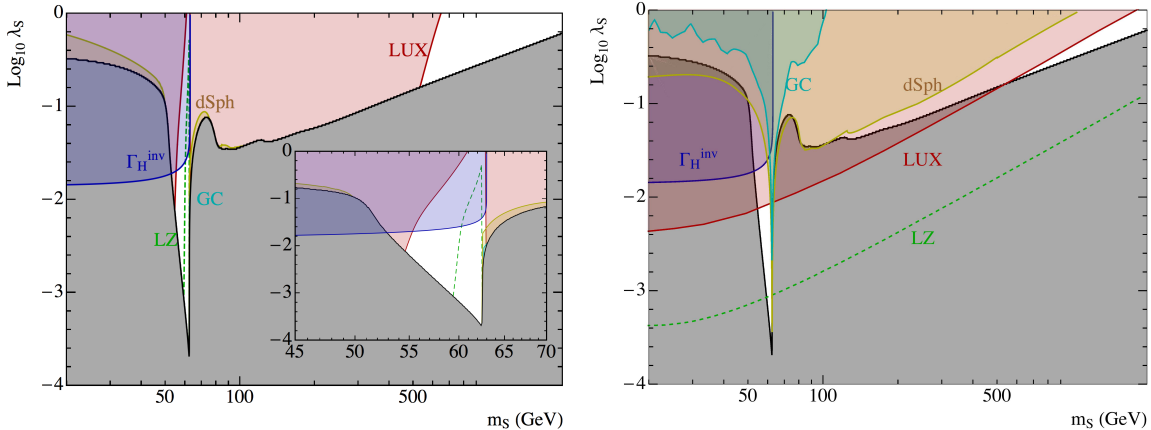


Figure 2: Excluded regions on the parameter space of the SHP model from different experimental constraints. The gray area (below the black line) is excluded since the relic density exceeds the Planck result. The blue area (labeled Γ_H^{inv}) is ruled out from the invisible Higgs width. The red area (LUX) is excluded by direct DM detection limits. Yellow (dSph) and cyan (GC) areas are excluded by indirect detection constraints on the continuum spectrum of gamma-rays (from dwarf Spheroidal galaxies) and monochromatic gamma-ray lines (from the Galactic Centre), respectively. The dashed green line represents the predicted reach of the future LZ detector. The left panel includes a scale factor, ξ , in the calculations while in the right plot it is assumed that some extra non-thermal effects amend the prediction for the relic density, so that $\xi = 1$.

observed one (see, e.g., Ref. [60]). Note that, since the value of ξ has been fixed, the areas excluded by indirect detection bounds now extend upwards.

In either case, the conclusion is that the combination of experimental constraints and the requirement of obtaining the correct relic abundance rules out a big and interesting portion of the viable parameter space of the Higgs portal (see Ref. [61] for a recent comprehensive study), leaving only the white areas in Fig. 2. Interestingly, as previous analyses have shown [62–65] there still remains a narrow window of S -masses in the Higgs-funnel region ($m_S \simeq m_h/2$) and, besides, there is a large allowed range for higher masses, $m_S \gtrsim 500$ GeV. Next generation experiments such as XENON1T [66] and, especially, LZ [67] (shown explicitly) will test completely the region of large DM masses and a large part of the narrow window at the Higgs-resonance. In particular, LZ could exclude the Higgs-portal scenario almost completely, or, hopefully, get a positive detection. The possibility of totally closing the Higgs-portal windows in the near future using complementary constraints from indirect detection has been analyzed in refs. [61, 62, 64].

Various solutions have been proposed in order to avoid experimental constraints in the SHP model. In general, in order to break the correlation between the relic abundance and

direct detection predictions, the model has to be extended. For example, the mediator (Higgs) sector can be enlarged with new scalars [68–70]. Non-linear Higgs portals [71] and high-dimensional operators in models with composite Higgs [72] have been considered as well. One can also extend the dark sector to include new particles charged under the SM gauge group, such as a doublet, a triplet, or a top-partner (see, e.g., [73–76]), or even consider multicomponent dark matter scenarios [70, 77–80]. More complex scenarios have also been analysed, where both the dark matter and mediator sectors are enlarged [81], for example, adding new portals related to neutrino physics [82–85]. There is also the possibility that the dark matter is a singlet-fermion, in which case the Higgs-portal interactions occur at the non-renormalizable level. Finally, one can consider changing the nature of the DM candidate, see for example Refs. [86, 87].

The goal of this paper is to consider and examine the most economical modification of the conventional SHP model that could escape the present and future searches, thus offering a viable (slightly modified) Higgs-portal scenario if a positive detection does not occur. The model consists of the addition of a second singlet scalar in the dark sector, which opens up new annihilation and coannihilation channels (previous work in this line has been carried out in Ref. [88]).

The article is organised as follows. The model is introduced in Section 2, where we explain how the correct relic abundance can be achieved for large regions of the parameter space. In Section 2.2, we describe the various experimental constraints to which the model is subject, and explain the way we have evaluated them. They include bounds from direct and indirect DM detection, the lifetime of the extra particle and the invisible decay of the Higgs boson. In Section 3 we perform a scan in the parameter space, explicitly showing that our model is viable for any DM mass above 50 GeV, thereby reopening the Higgs portal for scalar DM. In Section 4 we discuss the interpretation of this model in terms of an Effective Field Theory. Finally, the conclusions of our study are presented in Section 5. The Appendix is devoted to the calculation of the relevant radiative corrections for DM processes.

2 The extended singlet-scalar Higgs portal (ESHP)

The modification of the conventional SHP model that we consider consists simply of extending the DM sector with the addition of a second scalar. Denoting S_1 , S_2 the two scalar particles, and imposing a global Z_2 symmetry ($S_1 \rightarrow -S_1$, $S_2 \rightarrow -S_2$) in order to guarantee the

stability of the lightest one, the most general renormalizable Lagrangian reads

$$\begin{aligned} \mathcal{L}_{\text{ESHP}} = & \mathcal{L}_{\text{SM}} + \frac{1}{2} \sum_{i=1,2} \left[(\partial_\mu S_i)^2 - m_i^2 S_i^2 - \frac{1}{12} \lambda_{i4} S_i^4 \right] - \frac{1}{6} \lambda_{13} S_1 S_2^3 - \frac{1}{6} \lambda_{31} S_1^3 S_2 - \frac{1}{4} \lambda_{22} S_1^2 S_2^2 \\ & - \frac{1}{2} \lambda_1 S_1^2 |H|^2 - \frac{1}{2} \lambda_2 S_2^2 |H|^2 - \lambda_{12} S_1 S_2 \left(|H|^2 - \frac{v^2}{2} \right), \end{aligned} \quad (2.2)$$

where the subscript ESHP stands for “extended singlet-scalar Higgs portal”. The terms in the second line describe the DM/SM interactions, which occur through the Higgs sector. After EW breaking, $H^0 = (v + h)/\sqrt{2}$, there appear new terms, including trilinear terms between $S_{1,2}$ and the Higgs boson, such as $(\lambda_{12}v)hS_1S_2$. Stability constraints in this type of models have been studied in Ref. [89]. We have chosen S_1, S_2 to be the final mass eigenstates (after EW breaking), with physical masses, $m_{S_i}^2 = m_i^2 + \lambda_i v^2/2$, thus the form of the last term in eq.(2.2). From now on, S_1 will represent the lightest mass eigenstate of the dark sector, and thus the DM particle.

2.1 The relic density

The extra terms in the Lagrangian open up new ways of DM annihilation, illustrated in Fig. 3. These include processes mediated by S_2 (in t -channel) and co-annihilation processes. Besides, if S_1 and S_2 are in thermal equilibrium between them (thanks to the interaction terms in the first line of eq.(2.2)), the processes driving S_2 -annihilation contribute to the DM annihilation as well.

We are interested in the possibility that S_1 plays the role of DM, and that it reproduces the observed relic density while evading the bounds discussed in the previous section for the usual SHP model. Hence we will mainly focus in the regime where λ_1 (the equivalent to λ_S in the ordinary Higgs-portal) is small. As a matter of fact, λ_1 might be even vanishing, and the processes of Fig. 3 could still produce the necessary annihilation. However, this is not a natural choice from the point of view of quantum field theory. Since 1-loop diagrams with two λ_{12} vertices generate $S_1^2 |H|^2$ interactions, a conservative attitude is to assume that λ_1 is not smaller than $\sim \lambda_{12}^2/(4\pi)^2$. The same argument holds for λ_2 . Actually, for the sake of definiteness we will set $\lambda_2 = \lambda_{12}^2/(4\pi)^2$ through the paper.

Moreover, all the processes where a λ_1 -vertex is involved get new radiative corrections. In particular, the trilinear vertex (after EW breaking) $S_1 S_1 h$, which appears in DM annihilation and scattering processes (relevant for indirect and direct detection), has to be corrected by 1-loop diagrams, such as the ones depicted in Fig. 4. Due to the adopted smallness of λ_2 , other 1-loop diagrams are subdominant. Assuming for simplicity that λ_{31} (involved in the second diagram of Fig. 4) is of the same order as λ_{12} , all these contributions are $\mathcal{O}(\lambda_{12}^2/(4\pi)^2)$, which is precisely the smallest natural value for λ_1 . This means that only when λ_1 is close

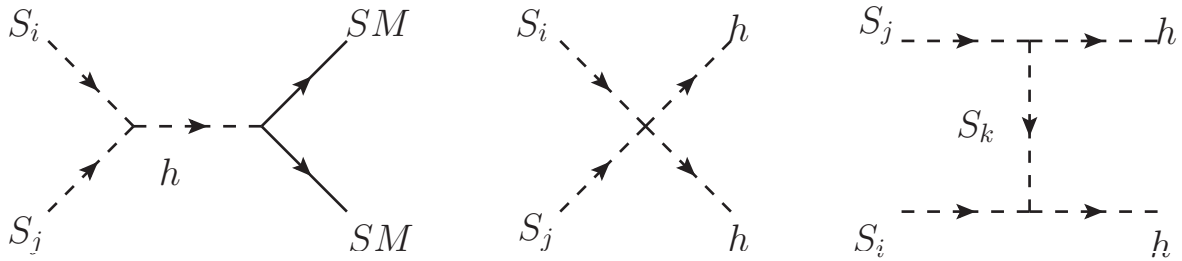


Figure 3: Extended Higgs-portal scenario (ESHP): annihilation processes involving particles of the dark sector, S_i , $i = 1, 2$.

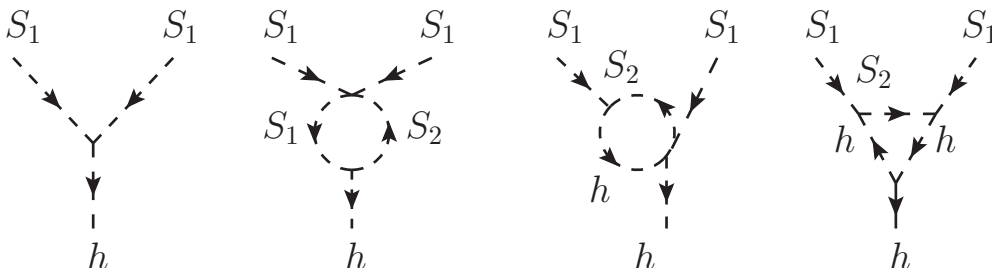


Figure 4: Tree-level $S_1 S_1 h$ vertex and main 1-loop corrections.

to this lower limit the contributions of these diagrams may be significant⁴. Nevertheless, for consistency, we have included the contribution of the 1-loop diagrams in all cases. A detailed discussion of these radiative corrections is given in the Appendix.

Let us now turn our attention to the computation of the relic density. We will start by considering a scenario in which λ_1 is as small as possible ($\lambda_1 = \lambda_{12}^2/(4\pi)^2$). Then, λ_1 can be neglected for all the relevant physical processes in most cases, so the only significant parameters to describe the DM physics are m_{S_1} , m_{S_2} , and λ_{12} . For each value of the DM mass, m_{S_1} , we are interested in finding out which combinations of m_{S_2} and λ_{12} lead to the correct relic density.

Fig. 5 shows the line along which the correct DM relic abundance is obtained for three representative cases, namely $m_{S_1} = 40, 60,$ and 200 GeV, i.e., below, around and above the Higgs resonance (left, middle and right panels, respectively). Let us discuss each case separately.

⁴In that case, there may be accidental cancellations between the tree-level and the radiative corrections, as can be checked from the explicit expressions given in the Appendix. Moreover these cancellations can be more or less significant depending on the external momenta entering the vertex. This opens the possibility of blind spots for direct or indirect detection, while keeping a sizable annihilation in the early universe.

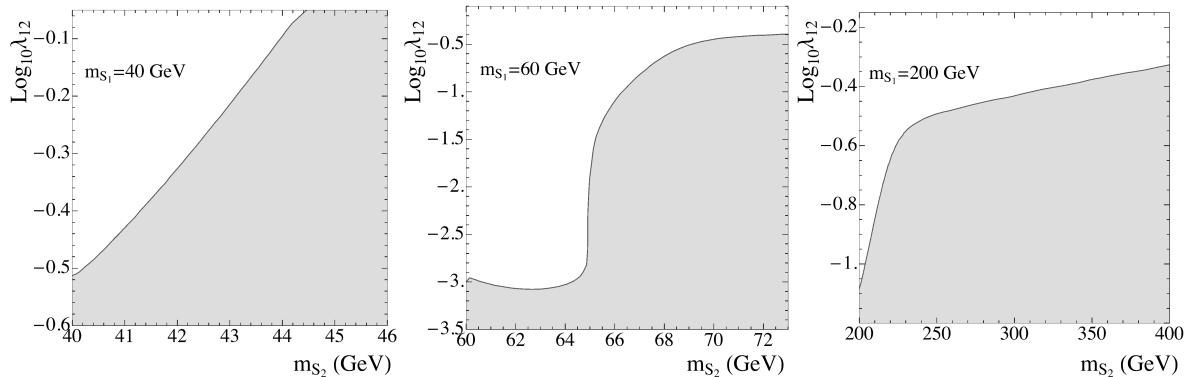


Figure 5: Range of values in the $\{\lambda_{12}, m_{S_2}\}$ plane leading to the correct DM relic density for three illustrative values of the DM mass: (from left to right) $m_{S_1} = 40$ GeV, 60 GeV, and 200 GeV. The DM-Higgs coupling has been fixed to $\lambda_1 = \lambda_{12}^2/(4\pi)^2$. The solid black line represents the Planck result. The grey area below this line is excluded since $\Omega_{S_1} > \Omega_{CDM}$.

For small DM masses (left panel), the correct relic density can be obtained through coannihilation effects with S_2 for a wide range of values of λ_{12} when $m_{S_2} - m_{S_1} \lesssim 5$ GeV. As m_{S_2} grows and departs from m_{S_1} , the required value of λ_{12} is larger and, at some point, it becomes non-perturbative.

When m_{S_1} is not far from the Higgs resonance (middle panel), we observe two different regimes. If $m_{S_1} + m_{S_2}$ is smaller than m_h , but such that $m_{S_1} + m_{S_2} \approx m_h$, the resonant condition for the s -channel $S_1 S_2 \rightarrow h \rightarrow SM SM$ can still be satisfied (S_1 and S_2 can have the correct energy due to their kinetic energy in the thermal bath) and the required value of λ_{12} is small.⁵ On the other hand, when $m_{S_1} + m_{S_2} > m_h$ the resonant effect is not possible. Consequently λ_{12} has to increase to reproduce the correct relic density. For sufficiently large m_{S_2} and λ_{12} , the corresponding value of the λ_1 coupling (which in this example is set to $\lambda_1 = (\lambda_{12}/4\pi)^2$) and the size of the 1-loop diagrams of Fig. 4 become large enough for the DM to be efficiently annihilated through the usual SHP process, $S_1 S_1 \rightarrow h \rightarrow SM SM$. In this regime, the model works essentially as the conventional SHP and the S_2 particle is irrelevant. Then the line in the plot becomes horizontal since the required value of λ_1 is related to that of λ_{12} through the above identification. However, the model could also work with essentially the same λ_1 and a smaller λ_{12} .

Finally, for $m_{S_1} > m_h/2$ (right panel), we can distinguish two regimes. When $m_{S_2} \sim m_{S_1}$, coannihilation effects are still present and the dependence with λ_{12} resembles that of the left

⁵Actually, it is quite independent of m_{S_2} , for the following reason. The amount of DM annihilated in this way is proportional to the product of two Boltzman factors: the one that suppresses the S_2 -density and the one that kinematically suppresses the $S_1 S_2 \rightarrow h$ process. As m_{S_2} increases, the first Boltzman factor decreases and the second one increases, keeping the product almost constant.

panel. However, for large m_{S_2} coannihilation effects are not effective and the relic density becomes less sensitive to m_{S_2} . In that case, if $m_{S_1} > m_h$ (as in the example of the figure), the t -channel diagram of Fig. 5, with S_1 in the external legs annihilating through S_2 -exchange into a pair of Higgs bosons, is kinematically accessible and it becomes the main contribution to the annihilation cross section.

2.2 Observational and experimental constraints

From the discussion in the previous subsection, it seems that for any value of m_{S_1} , we can suitably choose $\{m_{S_2}, \lambda_{12}\}$ to reproduce the correct relic density. Since λ_1 can be very small, one might expect that the ESHP model can evade easily the usual constraints on the singlet-scalar Higgs-portal.

However, this is not so straightforward. First, a sizable λ_{12} has potential impact on several observables, as we are about to see. Also, one must check that the existence of the second dark (unstable) species, S_2 , does not produce any cosmological disaster in the early universe. Finally, we might actually be interested in varying the value of λ_1 above its minimal value (in order to be as general as possible).

In this subsection we discuss the various physical constraints to which the model is subject.

Invisible width of the SM Higgs boson. From the observed decay channels of the SM Higgs boson, an experimental constraint can be derived on its invisible decay width. Namely, using the recent ATLAS and CMS results [53, 90–92], we will impose $\text{BR}(h \rightarrow \text{inv}) \leq 0.20$ (at a 90% confidence level) throughout this article. In the scenario presented here, the DM sector can contribute to the invisible width of the SM Higgs through the decays $h \rightarrow S_1 S_1$, $h \rightarrow S_1 S_2$, and $h \rightarrow S_2 S_2$, when these are kinematically allowed (see also Ref. [88]).

The corresponding decay widths at tree level read

$$\begin{aligned}
 \Gamma_{h \rightarrow S_1 S_1} &= \frac{\lambda_1^2 v^2}{32\pi m_h} \left(1 - \frac{4m_{S_1}^2}{m_h^2}\right)^{1/2}, \\
 \Gamma_{h \rightarrow S_1 S_2} &= \frac{\lambda_{12}^2 v^2}{64\pi m_h} \left(1 - \frac{(m_{S_2} + m_{S_1})^2}{m_h^2}\right)^{1/2} \left(1 - \frac{(m_{S_2} - m_{S_1})^2}{m_h^2}\right)^{1/2}, \\
 \Gamma_{h \rightarrow S_2 S_2} &= \frac{\lambda_2^2 v^2}{32\pi m_h} \left(1 - \frac{4m_{S_2}^2}{m_h^2}\right)^{1/2}.
 \end{aligned} \tag{2.3}$$

In our calculation, we have included the radiative corrections to the $S_1 S_1 h$ coupling (see Fig.4), as explained in the previous section. As mentioned in the Introduction, in the conventional SHP this constraint excludes areas with large coupling for small dark matter masses.

In the ESHP, both λ_1 and λ_2 can be chosen small and, therefore, $h \rightarrow S_1 S_2$ is the most relevant process, setting an upper bound on λ_{12} .

Lifetime of the extra scalar particle. The heavy scalar S_2 is unstable and decays into S_1 (plus SM products). We will require that the decay occurs before Big Bang nucleosynthesis, so as not to spoil its predictions. In fact, if S_2 is substantially heavier than S_1 , namely $m_{S_2} > m_{S_1} + m_h$, it rapidly decays as $S_2 \rightarrow S_1 h$ through the corresponding trilinear coupling λ_{12} . However, if $m_{S_2} < m_{S_1} + m_h$, we need to consider the three-body decay $S_2 \rightarrow S_1 f \bar{f}$. The latter is in general fast enough when the $S_1 b \bar{b}$ channel is open, but the lifetime of S_2 increases rapidly below this mass. We have computed the lifetime of S_2 using CalcHEP [93], and excluded points in the scan where $\tau_{S_2} > 1$ s.

Direct detection. The tree-level scattering of S_1 off quarks occurs via a t -channel Higgs exchange, as depicted in Fig. 6, where the gray circle represents the sum of the (tree-level and 1-loop) vertices of Fig. 4. Since λ_1 can be very small, the constraints from direct detection experiments are substantially alleviated, in contrast with the situation of the canonical Higgs portal, as has also been observed in Ref. [88].

We have explicitly computed the spin-independent contribution to the DM-nucleon elastic scattering cross section, $\sigma_{S_1 p}^{SI}$, which occurs through the exchange of a Higgs boson, as illustrated in Fig. 6. The Higgs-nucleon coupling can be parametrized as $f_N m_N / v$ where $m_N \simeq 0.946$ GeV is the mass of the nucleon. According to this, the spin-independent cross section, $\sigma_{S_1 p}^{SI}$, reads

$$\sigma_{S_1 p}^{SI} = \frac{\lambda_1^2 f_N^2 \mu^2 m_N^2}{4\pi m_h^4 m_{S_1}^2}, \quad (2.4)$$

where $\mu = m_N m_{S_1} / (m_N + m_{S_1})$ is the nucleon-DM reduced mass. The f_N parameter contains the nucleon matrix elements, and its full expression can be found, e.g., in ref. [62]. Using the values for the latter obtained from the lattice evaluation [94–99], one arrives at $f_N = 0.30 \pm 0.03$, in agreement with Ref. [62]. Finally, we have included one-loop contributions to the $S_1 S_1 h$ coupling, shown in Fig. 4, according to the computation given in the Appendix.

Then, we have implemented the most recent upper bounds obtained by the LUX collaboration [58] (which improves the bound obtained by PandaX-II [59]) for DM particles with masses above 6 GeV.⁶ Notice that since S_1 is a scalar field, there is no contribution to spin-dependent terms.

Although in principle we could also have inelastic scattering processes at tree level, $S_1 q \rightarrow$

⁶The SuperCDMS [100] and CRESST [101] collaborations have obtained more stringent constraints for light DM particles, but this range of masses is excluded in our model, mainly because of the experimental constraint on the invisible decay width of the Higgs boson.

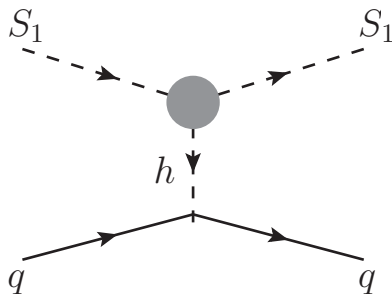


Figure 6: Diagrams contributing to the direct detection of S_1 . The gray circle represents the sum of the (tree-level and 1-loop) vertices of Fig. 4.

S_2q , the typical mass difference in our scenario is such that $m_{S_2} - m_{S_1} > 1$ GeV, significantly larger than the kinetic energy of the incoming DM particle (which is smaller than ~ 1 MeV for DM particles lighter than ~ 1 TeV), and this process does not take place.

Indirect detection Regarding indirect dark matter searches, the most relevant bounds for this model can be derived from gamma-ray searches from dwarf spheroidal galaxies (for the continuum spectrum) and the galactic centre (for gamma ray lines and spectral features).

In order to apply the dwarf spheroidal galaxies data on the continuum, we have computed the thermally-averaged annihilation cross section, $\langle\sigma v\rangle$, in the dwarf galaxies using MicrOMEGAs [102, 103], assuming that the initial particles are at rest (a good approximation since the velocity of the DM is low). We have then confronted the results with the combined analysis of Fermi-LAT and Magic [104], considering the upper bounds on $\langle\sigma v\rangle$ for annihilation into $b\bar{b}$ (again a good approximation since the annihilation is through the Higgs and this is the main final state when it is open).

On the other hand, for gamma ray lines in the galactic centre, we have calculated the annihilation cross section into a pair of photons, $\langle\sigma v\rangle_{\gamma\gamma}$, again using MicrOMEGAs, and confronted it with the upper bound given by Fermi-LAT [105]. We have chosen the Einasto [106, 107] profile for the DM halo, since is more restrictive than Navarro-Frenk-White (NFW) [108, 109] and has a good fit to results of numerical simulations. As in the SHP model, a Breit-Wigner enhancement near the Higgs resonance takes place,⁷ although, given the small decay width of the Higgs boson, it only occurs for a narrow range of masses. This leads to a sizable annihilation cross section in that region.

Finally, let us recall that indirect detection constraints are very sensitive to whether the gamma-ray flux is re-scaled by the dark matter density squared (ξ^2).

⁷This has been studied in various models [110–114].

3 Results

In this section we explore the parameter space of the ESHP model, incorporating all the experimental constraints and computing the theoretical predictions of observables for direct and indirect DM searches. As mentioned in the previous section, we have used MicrOMEGAs [102] to compute the relic abundance and indirect detection observables (the thermal average of the annihilation cross section of S_1 particles in the DM halo, $\langle\sigma v\rangle_0$, and the resulting gamma-ray flux). The spin independent S_1 -nucleon scattering cross section, $\sigma_{S_1 p}^{SI}$, and the invisible Higgs decay width, have been computed including one-loop corrections, as explained in Section 2.2.

In order to facilitate the comparison of the model with the usual SHP, we have carried out a series of numerical scans, for fixed values of λ_{12} , in the three dimensional parameter space $\{m_{S_1}, \lambda_1, m_{S_2}\}$, searching for points where S_1 is a viable candidate for dark matter. Note that the first two parameters are those of the SHP, i.e. the mass and quartic coupling of the DM. As already mentioned, we will set λ_2 at its lowest natural value, $\lambda_2 = \lambda_{12}^2/(4\pi)^2$. This is also the lower limit of λ_1 in the scans.

We have represented the results of the scans in Figs. 7 and 8, where $\{m_{S_1}, \lambda_1\}$ and $\{m_{S_1}, m_{S_2}\}$ are plotted for fixed values of λ_{12} . From top to bottom, we have chosen $\lambda_{12} = 0.01, 0.1, 1$, respectively, thereby gradually switching on the effect of the extra singlet in the model. The different experimental constraints are added sequentially from left to right. The left column includes the bounds from the invisible Higgs decay width and lifetime of S_2 . The central column incorporates indirect detection bounds from Fermi-LAT results on the Galactic Centre and dSphs. Finally, in the right column we add the direct detection limits from LUX. In all the plots, black dots correspond to those in which the (thermal) relic abundance of S_1 matches the results from the Planck satellite, whereas grey points are those in which S_1 is a subdominant dark matter component.

In all the plots of Fig. 7 an accumulation of black dots along a thick line is visible, which coincides with the relic-density line of the standard SHP (the black line of Fig. 2). For these points, the presence of the extra particle, S_2 , has no effect, because the λ_{12} coupling is too small or/and S_2 is substantially heavier than S_1 . These points appear as uniformly scattered in the $\{m_{S_1}, m_{S_2}\}$ plane in Fig. 8. Besides this (somehow trivial) thick line, there are new regions of interest, which we discuss below.

The results for the top row ($\lambda_{12} = 0.01$) resemble those of the usual SHP due to the smallness of λ_{12} . This can also be checked from the fact that the black dots in the plots in the first row of Fig. 8, appear uniformly scattered in the allowed regions. Consequently, the parameter space is extremely constrained by the combined effect of of the invisible Higgs width, indirect detection and (most notably) direct detection limits. Once all the bounds

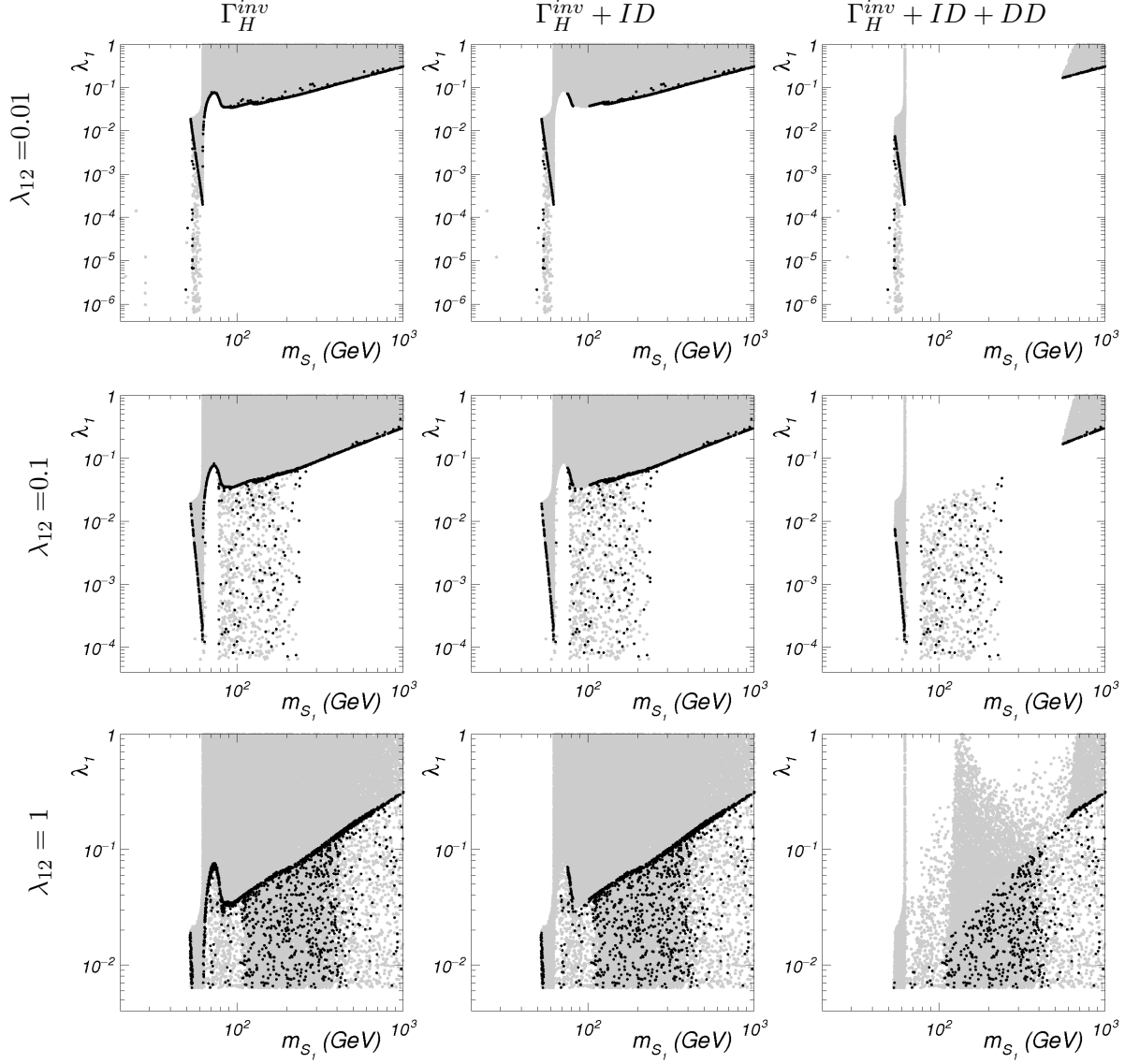


Figure 7: Effect of the experimental constraints in the $\{\lambda_1, m_{S_1}\}$ parameter space of the ESHP model. From up to down, we have fixed $\lambda_{12} = 0.01, 0.1, 1$, and $\lambda_2 = \lambda_{12}^2 / (4\pi)^2$. In all the plots, black (gray) points correspond to those where $\Omega h^2 = 0.119 \pm 0.003$ ($\Omega h^2 < 0.116$). The left column incorporates only constraints from lifetime of S_2 and invisible decay width of the Higgs boson. The central column includes also the indirect detection (dSph and gamma ray lines). Finally, the bottom row includes the bound from the LUX constraint.

are included, only the points in the Higgs resonance and those with $m_{S_1} > 500$ GeV survive. Still, when these results are compared to the left panel of Figure 2, we observe a new (small) population of points at the Higgs resonance, with very small values of the coupling λ_1 . This occurs when the masses of S_2 and S_1 are close enough so that coannihilation effects become

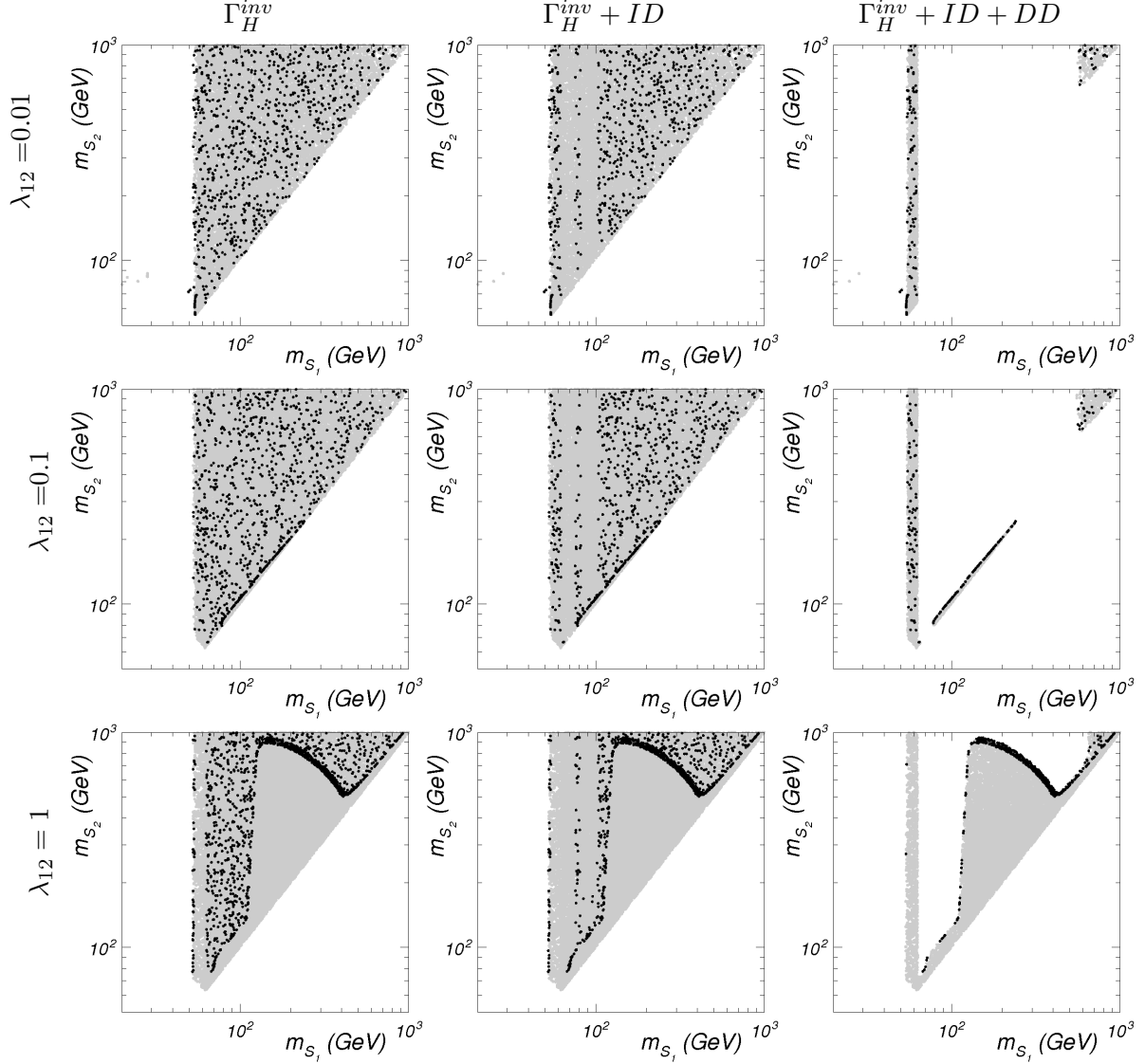


Figure 8: Effect of the experimental constraints in the $\{m_{S_1}, m_{S_2}\}$ parameter space of the ESHP model. We have used the same examples and colour conventions as in Fig. 7.

important (first diagram of Fig. 3). Away from the resonance region, the coannihilation effect is irrelevant due to the small size of λ_{12} assumed here, so the correct relic density is obtained only for the usual value of λ_1 , independently of how close m_{S_1} and m_{S_2} are.

As we increase the value of λ_{12} , new areas of the parameter space become available. In the middle row of Fig. 7, ($\lambda_{12} = 0.1$), we observe a region of black dots with masses $m_{S_1} \approx 100 - 200$ GeV and a very small λ_1 coupling. These points have the correct relic abundance thanks to coannihilation effects, which requires $m_{S_1} \sim m_{S_2}$. They can be observed in the second row of Fig. 8 as a thick line of black dots in that range of masses.

When $\lambda_{12} = 1$ (last row of Fig. 7), the effect of the DM annihilation in two Higgses, $S_1 S_1 \rightarrow hh$, exchanging S_2 in t -channel as in the last diagram of Fig. 3, becomes more remarkable, as soon as it is kinematically allowed, i.e. for $m_{S_1} \geq m_h$. This is the reason for the denser clouds of black dots out from the standard Higgs-portal thick line. For smaller values of m_{S_1} co-annihilation is still the main responsible for DM annihilation, thus requiring the S_1, S_2 masses to be closer. All this can be seen in Fig. 8. In the bottom panels of that figure we see that, for $m_{S_1} \leq m_h$, there is a thin “black line” made of points close to $m_{S_1} = m_{S_2}$. The short distance of this line to the perfect degeneracy shows the required closeness between m_{S_1} and m_{S_2} to produce the amount of co-annihilation that gives the observed relic density. Below that line co-annihilation is too strong, so there are only gray dots (too low relic density). For $m_{S_1} \geq m_h$ the line moves far away from $m_{S_1} = m_{S_2}$. As mentioned above, this behavior is due to the opening of the $S_1 S_1 \rightarrow hh$ process with both Higgses on-shell, which occurs via exchange of S_2 in t -channel (see Fig. 3). This process is very efficient, thus m_{S_2} has to get much larger to appropriately decrease its effect and keep the relic density at the right value. However, as m_{S_1} continues to increase, the black line again approaches $m_{S_2} \simeq m_{S_1}$. The reason is that the larger m_{S_1} the less efficient the annihilation process, an effect that must be compensated in the t -channel diagram by a larger λ_{12} or a smaller m_{S_2} ; and the latter is the only possibility since we have set $\lambda_{12} = 1$ in the plot. This can be easily understood by considering the t -channel diagram as generating an effective vertex, $S_1^2 h^2$, with strength $\lambda_{\text{eff}} \propto \lambda_{12}^2 / m_{S_2}^2$. In the next section we will elaborate more on this aspect.

As in the case of the conventional SHP model, we expect future direct detection experiments (and in particular LZ) to be able to test large areas of the parameter space of our extended, ESHP, scenario. We represent in Fig. 9 the theoretical predictions for the elastic scattering cross section of S_1 with protons, after all experimental constraints are applied. We indicate by means of a green line the expected reach of LZ. As we can observe, although a large area of the parameter space might be probed by these searches, there is a substantial region for which the predictions are beyond LZ sensitivity. For $\lambda_{12} = 0.1 - 1$, this is possible for a range of DM masses between 100 GeV and 1 TeV (besides the usual narrow region at the Higgs resonance for $m_{S_1} \simeq m_h/2$), while satisfying the constraint on the relic abundance. None of these points can be probed by indirect detection either.

4 Effective-theory description

As we have seen in the previous sections, the presence of the second particle, S_2 , in the dark sector can enable the efficient annihilation of the DM particle, S_1 , even if the usual quartic coupling of the latter, $\lambda_1 S_1^2 |H|^2$, is small enough to evade direct and indirect detection

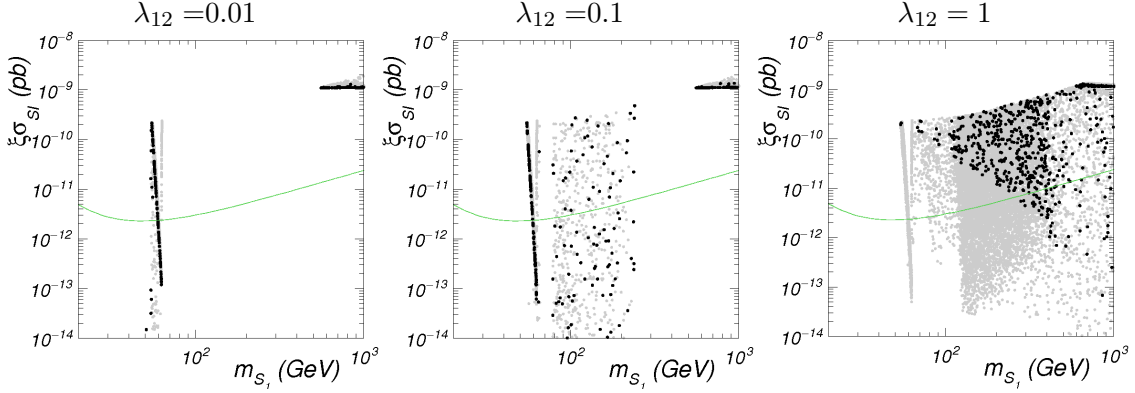


Figure 9: Spin-independent scattering cross section of S_1 with protons as a function of its mass in the ESHP model. From left to right, we have fixed $\lambda_{12} = 0.01, 0.1, 1$, and 1 , respectively.

constraints.

Since $m_{S_2} > m_{S_1}$, one can wonder whether S_2 might be integrated-out. Then, one would be left with a usual Higgs-portal scenario with just one particle, S_1 , plus some higher-order operators, involving S_1 and H . If this procedure is sound, these additional operators should be “clever” enough to mimic the effects of the heavy particle, S_2 . Actually, the possibility of opening the allowed parameter-space of the Higgs-portal by adding new operators in the spirit of an effective field theory (EFT) has been considered in refs. [71, 72]. In our case, the coefficients of the EFT expansion are not completely independent, since they are determined by the ultraviolet (UV) completion, i.e., the Lagrangian of eq.(2.2). As we are about to see, this produces a quite special EFT, which is indeed very efficient in rescuing the excluded regions of the usual Higgs-portal for singlet scalar DM. Without the knowledge of the UV completion, such EFT could be seen as designed ad hoc for that purpose.

In fact, it is not always possible to mimic the effects of S_2 by integrating it out in some approximation. In particular, when $m_{S_2} \simeq m_{S_1}$, such integration is not appropriate. Consequently, the EFT description is not suitable to describe the regions of the parameter space where co-annihilation effects are dominant, e.g., for $\lambda_{12} \lesssim 0.1$, see Figs.7 and 8. However, there are other regimes in which S_2 is substantially (though not enormously) heavier than S_1 , see for example Fig. 5 and the bottom row of Fig. 8. In those cases the EFT captures, at least qualitatively, the relevant physics.

Once S_2 is integrated out at tree-level from eq.(2.2), the relevant new terms in the effective Lagrangian are

$$\Delta\mathcal{L}_{\text{eff}}(S_1, H) = -\frac{1}{2} \frac{\lambda_{12}^2}{m_{S_2}^2} S_1^2 \left(|H|^2 - \frac{v^2}{2} \right)^2 + \dots \quad (4.5)$$

Of course, this operator arises from the third tree-level diagram in Fig. 3, with S_2 exchanged

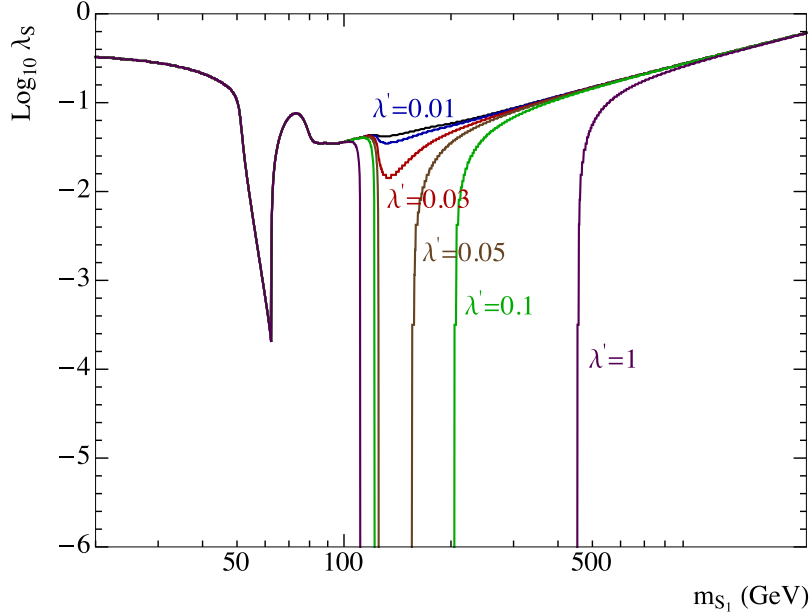


Figure 10: Contour lines of the correct relic DM abundance in an SHP effective theory consisting of the usual SHP Lagrangian plus an extra operator, as given in Eq. (4.6), for several values of the λ' coupling. This effective theory describes the ESHP in large regions of the parameter space.

in t -channel. Here the dots stand for higher order terms in S_1 or H . An important property of $\Delta\mathcal{L}_{\text{eff}}$ is that, after EW breaking, the operator (4.5) has the form $\frac{1}{4}S_1^2(h^2+2vh)^2$, triggering a contribution to the $S_1^2h^2$ quartic coupling, without generating new cubic couplings, S_1^2h (as a usual quartic coupling does). This is extremely useful to enhance the S_1 annihilation without contributing to direct-detection processes or to the Higgs invisible-width (if S_1 is light enough).

Fig. 10 shows the performance of this Higgs-portal scenario with the presence of such extra operator, which we have parametrized as

$$\mathcal{L}'_{\text{SHP}} = \mathcal{L}_{\text{SHP}} - \frac{1}{2} \frac{\lambda'}{m_{S_1}^2} S_1^2 \left(|H|^2 - \frac{v^2}{2} \right)^2, \quad (4.6)$$

where \mathcal{L}_{SHP} is the SHP Lagrangian, defined in equation (1.1), and $\lambda' = \lambda_{12}^2 (m_{S_1}/m_{S_2})^2$. The lines shown in the $\{\lambda_S, m_{S_1}\}$ plane correspond to the correct relic abundance for different values of the effective coupling λ' . As we can observe, the contribution from the effective operator triggers on when the annihilation channel into a pair of Higgs bosons gets kinematically allowed. Then, for a given value of m_{S_1} , as λ' increases, the value of λ_S needed to recover the correct relic abundance decreases, eventually becoming irrelevant. For larger values of the DM mass, the effective operator becomes less efficient and eventually we recover

the original behaviour. If we demand that $\lambda' < 1$, then the contribution from the effective operator is important for DM masses between 126 GeV and approximately 500 GeV. In this range of masses, the usual quartic coupling λ_S can be very small, thus helping to evade direct-detection limits.

In other words, in this region of DM masses, for any value of the λ_S coupling, there exists a value of λ' that allows to recover the correct relic density. Since $\lambda' = \lambda_{12}^2 (m_{S_1}/m_{S_2})^2$, there are many combinations of the two underlying parameters of the U.V. theory, $\{\lambda_{12}, m_{S_2}\}$, leading to the correct result. These findings are in good agreement with the results presented in the previous section (Fig. 7), in particular with those for large λ_{12} in the region of m_{S_1} , where the co-annihilation effects are not dominant.

5 Conclusions

One of the most economical and explored models of dark matter (DM) is the so-called singlet-scalar Higgs portal (SHP) model. It simply consists of an extra singlet scalar field (the DM particle), which is minimally coupled to the SM through interactions with the ordinary Higgs at the renormalizable level. Unfortunately, the experimental advances in direct and indirect dark matter searches, together with the latest results from the LHC, have ruled out vast areas of the viable parameter space of this scenario. Moreover, it is expected that future experiments will completely probe it within the next years and rule it out if no signal is found.

Motivated by the appealing simplicity of this model, we have considered in this article a minimal extension (ESHP) that could evade detection. It consists of the addition of an extra real singlet scalar field in the dark sector, coupled also in a minimal, renormalizable way.

We show that the new annihilation and/or co-annihilation channels involving the extra singlet allow to reproduce the correct relic abundance, even if the usual interaction of the DM particle with the Higgs were arbitrarily small. This allows to easily avoid the bounds from direct and indirect DM searches.

Apart from the DM mass and its coupling to the Higgs, in its simplest version, the ESHP model has just two extra (relevant) parameters: the mass of the extra scalar and the quartic coupling between it, the DM particle and the Higgs field. Actually, the usual DM-Higgs coupling becomes irrelevant in most cases, since it is unnecessary, so the model has very few parameters. This permits to explore its phenomenology in an efficient way. In fact, though much more viable than the usual SHP model, this extended scenario is subject to a number of phenomenological constraints, most of them stemming from the mentioned quartic coupling between the DM, the extra scalar and the Higgs. These include bounds from the invisible width of the SM Higgs boson, the lifetime of the extra scalar particle, and direct and indirect

searches for DM. Still, large portions of the parameter space survive all (present and even future) constraints.

We have also shown that, in the regions where the main extra effect is the annihilation of DM particles into SM particles (essentially Higgses), through the interchange in t -channel of the extra particle, the latter can be integrated-out, leaving a “clever” SHP effective theory (just involving the DM particle and the Higgs) which can reproduce the relic density, while avoiding the usual strong constraints from DM searches. This is not possible however in the regions where the main extra effect is co-annihilation between the DM and the extra particle.

A Radiative contributions to the $S_1 S_1 h$ vertex

In this appendix we compute the dominant radiative contributions for relevant physical processes involving DM in the context of the ESHP model, defined by the Lagrangian of eq.(2.2). We will do it in the framework of the EW-broken theory.

Assuming for simplicity and convenience a small λ_2 coupling, as has been done throughout the paper, the most important radiative corrections are those contributing to the $S_1 S_1 h$ vertex, in particular the three 1-loop diagrams depicted in Fig. 4. This vertex plays a crucial role for a number of DM processes; namely DM annihilation in the early universe, direct and indirect DM detection, and contributions to the invisible width of the Higgs boson. Other relevant DM processes, in particular $S_1 S_1 \rightarrow hh$, receive radiative corrections as well, but they are much smaller than the contribution from the tree-level diagram in which a S_2 particle is exchanged in t -channel, see Fig. 3.

Therefore, in order to evaluate radiative corrections, the relevant terms of the Lagrangian in the broken phase are

$$\mathcal{L} \supset -\frac{1}{4!}\lambda h^4 - \frac{1}{3!}\lambda_1 v h^3 - \frac{1}{2}\lambda_{12} S_1 S_2 h^2 - \lambda_{12} v S_1 S_2 h - \frac{1}{3!}\lambda_{31} S_1^3 S_2 . \quad (\text{A.1})$$

In the following we will compute them, using the conventions of Ref. [115] for Feynman rules.

Let us start with the one-loop diagrams involving two propagators (second and third diagrams of Fig. 4). Their contribution to the vertex is given by

$$\frac{iv}{16\pi^2} \left[\lambda_{31} \lambda_{12} B_0(p_h^2; m_{S_1}, m_{S_2}) + \lambda_{12}^2 \left(B_0(p_{S_1}^2; m_{S_2}, m_h) + B_0(p_{S_1'}^2; m_{S_2}, m_h) \right) \right] , \quad (\text{A.2})$$

where p_{S_1} and $p_{S_1'}$ represent the momenta of the two S_1 particles entering the vertex, and

$$B_0(p^2, m_1, m_2) = (\text{Divergent part}) + \mathcal{B}(p^2, m_1, m_2) , \quad (\text{A.3})$$

with

$$\mathcal{B}(p^2, m_1, m_2) = - \int_0^1 dx \log \frac{xm_1^2 + (1-x)m_2^2 - x(1-x)p^2}{m_1 m_2} . \quad (\text{A.4})$$

In our case, the divergent part and the momentum-independent piece of $\mathcal{B}(p^2, m_1, m_2)$ can be absorbed in the renormalized value of λ_1 . Moreover, $\mathcal{B}(p^2, m_1, m_2)$ can be expanded in powers of the momentum, as

$$\mathcal{B}(p^2, m_1, m_2) = 1 - \frac{m_1^2 + m_2^2}{m_1^2 - m_2^2} \log \frac{m_1}{m_2} + p^2 F(m_1, m_2) + \mathcal{O}(p^4), \quad (\text{A.5})$$

with

$$F(m_1, m_2) = \frac{m_1^4 - m_2^4 - 2m_1^2 m_2^2 \log \frac{m_1^2}{m_2^2}}{2(m_1^2 - m_2^2)^3}. \quad (\text{A.6})$$

Keeping just the term proportional to p^2 turns out to be a good approximation in most cases (recall here that the p -independent terms in Eq. (A.5) are absorbed in a finite renormalization of λ_1). Hence a good approximation for the contribution to the $S_1 S_1 h$ vertex from the one-loop diagrams involving two propagators is

$$\Gamma^{(2)} \simeq \frac{iv}{16\pi^2} \left[\lambda_{31} \lambda_{12} p_h^2 F(m_{S_1}, m_{S_2}) + \lambda_{12}^2 (p_{S_1}^2 + p_{S_1'}^2) F(m_{S_2}, m_h) \right]. \quad (\text{A.7})$$

Alternatively, this contribution to the vertex can be viewed as the Feynman rule stemming from the corresponding term in the effective action, namely

$$16\pi^2 \Delta^{(2)} \mathcal{L} = -\frac{1}{2} \lambda_{31} \lambda_{12} v F(m_{S_1}, m_{S_2}) S^2 \partial^2 h - \lambda_{12}^2 v F(m_{S_2}, m_h) S (\partial^2 S) h. \quad (\text{A.8})$$

This is a convenient way to encode these contributions in the MicrOMEGAs code, as we have done throughout the paper.

Let us now consider the one-loop diagrams involving three propagators (fourth diagram of Fig. 4). The main difference with the previous two diagrams is that this represents a finite contribution which should be entirely counted, even the momentum-independent contribution, since the latter corresponds to a $S_1^2 |H|^4$ operator in the unbroken theory and cannot be absorbed in a finite renormalization of λ_1 . Using the same momentum expansion as before, the corresponding contribution to the $S_1 S_1 h$ vertex reads

$$\Gamma^{(3)} \simeq \frac{i}{16\pi^2} \lambda_{12}^2 \lambda v^3 \left[F_3(m_{S_2}, m_h, m_h) \right. \quad (\text{A.9})$$

$$\left. + (p_{S_1}^2 + p_{S_1'}^2) G(m_{S_2}, m_h, m_h) + p_h^2 G(m_h, m_h, m_{S_2}) \right], \quad (\text{A.10})$$

with

$$\begin{aligned}
F_3(m_1, m_1, m_2) &= -\frac{m_1^2 - m_2^2 - m_2^2 \log \frac{m_1^2}{m_2^2}}{(m_1^2 - m_2^2)^2}, \\
G(m_1, m_1, m_2) &= -\frac{m_1^6 - 6m_1^4 m_2^2 + 3m_1^2 m_2^4 + 2m_2^6 + 6m_1^2 m_2^4 \log \left(\frac{m_1^2}{m_2^2} \right)}{12m_1^2 (m_1^2 - m_2^2)^4}, \\
G(m_1, m_2, m_1) &= -\frac{m_1^4 + 4m_1^2 m_2^2 - 5m_2^4 - 2m_2^2 (2m_1^2 + m_2^2) \log \left(\frac{m_1^2}{m_2^2} \right)}{4(m_1^2 - m_2^2)^4}.
\end{aligned} \tag{A.11}$$

The corresponding terms in the effective action read

$$\begin{aligned}
16\pi^2 \Delta^{(3)} \mathcal{L} &= \frac{1}{2} \lambda_{12}^2 \lambda v^3 \left[F_3(m_{S_2}, m_h, m_h) S^2 h \right. \\
&\quad \left. - 2G(m_{S_2}, m_h, m_h) S (\partial^2 S) h - G(m_h, m_h, m_{S_2}) S^2 \partial^2 h \right].
\end{aligned} \tag{A.12}$$

Acknowledgements

This work has been partially supported by the MICINN / MINECO, Spain, under contracts FPA2013-44773-P, FPA2015-65929-P and FPA2016-78022-P. We also thank the Spanish MINECO Centro de excelencia Severo Ochoa Program under grant SEV-2012-0249, the Consolider-Ingenio CPAN CSD2007-00042, as well as MULTIDARK CSD2009-00064. D.G.C acknowledges support from the STFC and the partial support of the Centro de Excelencia Severo Ochoa Program through the IFT-UAM/CSIC Associate programme. The work of J.Q. is supported through the Spanish FPI grant SVP-2014-068899. J.Q. thanks Sandra Robles for her invaluable help with computational resources.

References

- [1] V. Silveira and A. Zee, *Scalar Phantoms*, *Phys. Lett.* **B161** (1985) 136–140.
- [2] J. McDonald, *Gauge singlet scalars as cold dark matter*, *Phys. Rev.* **D50** (1994) 3637–3649, [[hep-ph/0702143](#)].
- [3] C. P. Burgess, M. Pospelov and T. ter Veldhuis, *The Minimal model of nonbaryonic dark matter: A Singlet scalar*, *Nucl. Phys.* **B619** (2001) 709–728, [[hep-ph/0011335](#)].
- [4] H. Davoudiasl, R. Kitano, T. Li and H. Murayama, *The New minimal standard model*, *Phys. Lett.* **B609** (2005) 117–123, [[hep-ph/0405097](#)].

- [5] V. Barger, P. Langacker, M. McCaskey, M. J. Ramsey-Musolf and G. Shaughnessy, *LHC Phenomenology of an Extended Standard Model with a Real Scalar Singlet*, *Phys. Rev.* **D77** (2008) 035005, [0706.4311].
- [6] R. N. Lerner and J. McDonald, *Gauge singlet scalar as inflaton and thermal relic dark matter*, *Phys. Rev.* **D80** (2009) 123507, [0909.0520].
- [7] B. Grzadkowski and J. Wudka, *Pragmatic approach to the little hierarchy problem: the case for Dark Matter and neutrino physics*, *Phys. Rev. Lett.* **103** (2009) 091802, [0902.0628].
- [8] PLANCK collaboration, P. A. R. Ade et al., *Planck 2015 results. XIII. Cosmological parameters*, *Astron. Astrophys.* **594** (2016) A13, [1502.01589].
- [9] B. Feldstein, A. L. Fitzpatrick and E. Katz, *Form Factor Dark Matter*, *JCAP* **1001** (2010) 020, [0908.2991].
- [10] S. Chang, A. Pierce and N. Weiner, *Using the Energy Spectrum at DAMA/LIBRA to Probe Light Dark Matter*, *Phys. Rev.* **D79** (2009) 115011, [0808.0196].
- [11] K. R. Dienes, J. Kumar, B. Thomas and D. Yaylali, *Overcoming Velocity Suppression in Dark-Matter Direct-Detection Experiments*, *Phys. Rev.* **D90** (2014) 015012, [1312.7772].
- [12] J. Fan, M. Reece and L.-T. Wang, *Non-relativistic effective theory of dark matter direct detection*, *JCAP* **1011** (2010) 042, [1008.1591].
- [13] J. B. Dent, B. Dutta, J. L. Newstead and L. E. Strigari, *Effective field theory treatment of the neutrino background in direct dark matter detection experiments*, *Phys. Rev.* **D93** (2016) 075018, [1602.05300].
- [14] V. Gluscevic, M. I. Gresham, S. D. McDermott, A. H. G. Peter and K. M. Zurek, *Identifying the Theory of Dark Matter with Direct Detection*, *JCAP* **1512** (2015) 057, [1506.04454].
- [15] J. Kumar and D. Marfatia, *Matrix element analyses of dark matter scattering and annihilation*, *Phys. Rev.* **D88** (2013) 014035, [1305.1611].
- [16] C. Savage, G. Gelmini, P. Gondolo and K. Freese, *Compatibility of DAMA/LIBRA dark matter detection with other searches*, *JCAP* **0904** (2009) 010, [0808.3607].
- [17] J. Billard, L. Strigari and E. Figueroa-Feliciano, *Implication of neutrino backgrounds on the reach of next generation dark matter direct detection experiments*, *Phys. Rev.* **D89** (2014) 023524, [1307.5458].

- [18] X.-G. He, T. Li, X.-Q. Li, J. Tandean and H.-C. Tsai, *Constraints on Scalar Dark Matter from Direct Experimental Searches*, *Phys. Rev.* **D79** (2009) 023521, [0811.0658].
- [19] M. Farina, D. Pappadopulo and A. Strumia, *CDMS stands for Constrained Dark Matter Singlet*, *Phys. Lett.* **B688** (2010) 329–331, [0912.5038].
- [20] A. Bandyopadhyay, S. Chakraborty, A. Ghosal and D. Majumdar, *Constraining Scalar Singlet Dark Matter with CDMS, XENON and DAMA and Prediction for Direct Detection Rates*, *JHEP* **11** (2010) 065, [1003.0809].
- [21] X.-G. He and J. Tandean, *New LUX and PandaX-II Results Illuminating the Simplest Higgs-Portal Dark Matter Models*, *JHEP* **12** (2016) 074, [1609.03551].
- [22] V. Bonnivard, C. Combet, D. Maurin and M. G. Walker, *Spherical Jeans analysis for dark matter indirect detection in dwarf spheroidal galaxies - Impact of physical parameters and triaxiality*, *Mon. Not. Roy. Astron. Soc.* **446** (2015) 3002–3021, [1407.7822].
- [23] K. Ichikawa, M. N. Ishigaki, S. Matsumoto, M. Ibe, H. Sugai and K. Hayashi, *Foreground effect on the J-factor estimation of classical dwarf spheroidal galaxies*, 1608.01749.
- [24] N. Klop, F. Zandanel, K. Hayashi and S. Ando, *Impact of axisymmetric mass models for dwarf spheroidal galaxies on indirect dark matter searches*, 1609.03509.
- [25] S. Ipek, D. McKeen and A. E. Nelson, *A Renormalizable Model for the Galactic Center Gamma Ray Excess from Dark Matter Annihilation*, *Phys. Rev.* **D90** (2014) 055021, [1404.3716].
- [26] T. Daylan, D. P. Finkbeiner, D. Hooper, T. Linden, S. K. N. Portillo, N. L. Rodd et al., *The characterization of the gamma-ray signal from the central Milky Way: A case for annihilating dark matter*, *Phys. Dark Univ.* **12** (2016) 1–23, [1402.6703].
- [27] D. Hooper and L. Goodenough, *Dark Matter Annihilation in The Galactic Center As Seen by the Fermi Gamma Ray Space Telescope*, *Phys. Lett.* **B697** (2011) 412–428, [1010.2752].
- [28] D. Hooper and T. Linden, *On The Origin Of The Gamma Rays From The Galactic Center*, *Phys. Rev.* **D84** (2011) 123005, [1110.0006].
- [29] L. Goodenough and D. Hooper, *Possible Evidence For Dark Matter Annihilation In The Inner Milky Way From The Fermi Gamma Ray Space Telescope*, 0910.2998.

- [30] K. N. Abazajian and M. Kaplinghat, *Detection of a Gamma-Ray Source in the Galactic Center Consistent with Extended Emission from Dark Matter Annihilation and Concentrated Astrophysical Emission*, *Phys. Rev.* **D86** (2012) 083511, [1207.6047].
- [31] C. Gordon and O. Macias, *Dark Matter and Pulsar Model Constraints from Galactic Center Fermi-LAT Gamma Ray Observations*, *Phys. Rev.* **D88** (2013) 083521, [1306.5725].
- [32] FERMI-LAT collaboration, M. Ajello et al., *Fermi-LAT Observations of High-Energy γ -Ray Emission Toward the Galactic Center*, *Astrophys. J.* **819** (2016) 44, [1511.02938].
- [33] A. Berlin, D. Hooper and G. Krnjaic, *Thermal Dark Matter From A Highly Decoupled Sector*, *Phys. Rev.* **D94** (2016) 095019, [1609.02555].
- [34] A. De Simone, G. F. Giudice and A. Strumia, *Benchmarks for Dark Matter Searches at the LHC*, *JHEP* **06** (2014) 081, [1402.6287].
- [35] D. Hooper, C. Kelso and F. S. Queiroz, *Stringent and Robust Constraints on the Dark Matter Annihilation Cross Section From the Region of the Galactic Center*, *Astropart. Phys.* **46** (2013) 55–70, [1209.3015].
- [36] FERMI-LAT collaboration, M. Ackermann et al., *Searching for Dark Matter Annihilation from Milky Way Dwarf Spheroidal Galaxies with Six Years of Fermi Large Area Telescope Data*, *Phys. Rev. Lett.* **115** (2015) 231301, [1503.02641].
- [37] G. Giesen, M. Boudaud, Y. Génolini, V. Poulin, M. Cirelli, P. Salati et al., *AMS-02 antiprotons, at last! Secondary astrophysical component and immediate implications for Dark Matter*, *JCAP* **1509** (2015) 023, [1504.04276].
- [38] M. Cirelli and G. Giesen, *Antiprotons from Dark Matter: Current constraints and future sensitivities*, *JCAP* **1304** (2013) 015, [1301.7079].
- [39] A. Berlin, D. Hooper and S. D. McDermott, *Simplified Dark Matter Models for the Galactic Center Gamma-Ray Excess*, *Phys. Rev.* **D89** (2014) 115022, [1404.0022].
- [40] M. Duerr, P. Fileviez Pérez and J. Smirnov, *Gamma-Ray Excess and the Minimal Dark Matter Model*, *JHEP* **06** (2016) 008, [1510.07562].
- [41] A. Beniwal, F. Rajec, C. Savage, P. Scott, C. Weniger, M. White et al., *Combined analysis of effective Higgs portal dark matter models*, *Phys. Rev.* **D93** (2016) 115016, [1512.06458].

- [42] S. Profumo, L. Ubaldi and C. Wainwright, *Singlet Scalar Dark Matter: monochromatic gamma rays and metastable vacua*, *Phys. Rev.* **D82** (2010) 123514, [1009.5377].
- [43] F. S. Sage and R. Dick, *Gamma ray signals of the annihilation of Higgs-portal singlet dark matter*, **1604.04589**.
- [44] M. Duerr, P. Fileviez Perez and J. Smirnov, *Scalar Singlet Dark Matter and Gamma Lines*, *Phys. Lett.* **B751** (2015) 119–122, [1508.04418].
- [45] A. Cuoco, B. Eiteneuer, J. Heisig and M. Kraemer, *A global fit of the γ -ray galactic center excess within the scalar singlet Higgs portal model*, *JCAP* **1606** (2016) 050, [1603.08228].
- [46] C. Balázs and T. Li, *Simplified Dark Matter Models Confront the Gamma Ray Excess*, *Phys. Rev.* **D90** (2014) 055026, [1407.0174].
- [47] M. Duerr, P. Fileviez Pérez and J. Smirnov, *Scalar Dark Matter: Direct vs. Indirect Detection*, *JHEP* **06** (2016) 152, [1509.04282].
- [48] H. Han and S. Zheng, *Higgs-portal Scalar Dark Matter: Scattering Cross Section and Observable Limits*, *Nucl. Phys.* **B914** (2017) 248–256, [1510.06165].
- [49] J. Kozaczuk and T. A. W. Martin, *Extending LHC Coverage to Light Pseudoscalar Mediators and Coy Dark Sectors*, *JHEP* **04** (2015) 046, [1501.07275].
- [50] X.-G. He, T. Li, X.-Q. Li and H.-C. Tsai, *Scalar dark matter effects in Higgs and top quark decays*, *Mod. Phys. Lett.* **A22** (2007) 2121–2129, [hep-ph/0701156].
- [51] A. Djouadi, A. Falkowski, Y. Mambrini and J. Quevillon, *Direct Detection of Higgs-Portal Dark Matter at the LHC*, *Eur. Phys. J.* **C73** (2013) 2455, [1205.3169].
- [52] N. Craig, H. K. Lou, M. McCullough and A. Thalappilil, *The Higgs Portal Above Threshold*, *JHEP* **02** (2016) 127, [1412.0258].
- [53] CMS collaboration, V. Khachatryan et al., *Searches for invisible decays of the Higgs boson in pp collisions at $\sqrt{s} = 7, 8, \text{ and } 13 \text{ TeV}$* , *Submitted to: JHEP* (2016) , [1610.09218].
- [54] P. Ko and H. Yokoya, *Search for Higgs portal DM at the ILC*, *JHEP* **08** (2016) 109, [1603.04737].
- [55] H. Han, J. M. Yang, Y. Zhang and S. Zheng, *Collider Signatures of Higgs-portal Scalar Dark Matter*, *Phys. Lett.* **B756** (2016) 109–112, [1601.06232].

- [56] L. Carpenter, A. DiFranzo, M. Mulhearn, C. Shimmin, S. Tulin and D. Whiteson, *Mono-Higgs-boson: A new collider probe of dark matter*, *Phys. Rev.* **D89** (2014) 075017, [1312.2592].
- [57] M. Benito, N. Bernal, N. Bozorgnia, F. Calore and F. Iocco, *Particle Dark Matter Constraints: the Effect of Galactic Uncertainties*, 1612.02010.
- [58] LUX collaboration, D. S. Akerib et al., *Results from a search for dark matter in the complete LUX exposure*, *Phys. Rev. Lett.* **118** (2017) 021303, [1608.07648].
- [59] PANDAX-II collaboration, A. Tan et al., *Dark Matter Results from First 98.7 Days of Data from the PandaX-II Experiment*, *Phys. Rev. Lett.* **117** (2016) 121303, [1607.07400].
- [60] G. B. Gelmini and P. Gondolo, *Neutralino with the right cold dark matter abundance in (almost) any supersymmetric model*, *Phys. Rev.* **D74** (2006) 023510, [hep-ph/0602230].
- [61] M. Escudero, A. Berlin, D. Hooper and M.-X. Lin, *Toward (Finally!) Ruling Out Z and Higgs Mediated Dark Matter Models*, *JCAP* **1612** (2016) 029, [1609.09079].
- [62] J. M. Cline, K. Kainulainen, P. Scott and C. Weniger, *Update on scalar singlet dark matter*, *Phys. Rev.* **D88** (2013) 055025, [1306.4710].
- [63] F. S. Queiroz and K. Sinha, *The Poker Face of the Majoron Dark Matter Model: LUX to keV Line*, *Phys. Lett.* **B735** (2014) 69–74, [1404.1400].
- [64] L. Feng, S. Profumo and L. Ubaldi, *Closing in on singlet scalar dark matter: LUX, invisible Higgs decays and gamma-ray lines*, *JHEP* **03** (2015) 045, [1412.1105].
- [65] H. Wu and S. Zheng, *Scalar Dark Matter: Real vs Complex*, 1610.06292.
- [66] XENON collaboration, E. Aprile et al., *Physics reach of the XENON1T dark matter experiment*, *JCAP* **1604** (2016) 027, [1512.07501].
- [67] LZ collaboration, D. S. Akerib et al., *LUX-ZEPLIN (LZ) Conceptual Design Report*, 1509.02910.
- [68] K. Ishiwata, *Dark Matter in Classically Scale-Invariant Two Singlets Standard Model*, *Phys. Lett.* **B710** (2012) 134–138, [1112.2696].
- [69] A. Abada, D. Ghaffor and S. Nasri, *A Two-Singlet Model for Light Cold Dark Matter*, *Phys. Rev.* **D83** (2011) 095021, [1101.0365].

- [70] K. P. Modak, D. Majumdar and S. Rakshit, *A Possible Explanation of Low Energy γ -ray Excess from Galactic Centre and Fermi Bubble by a Dark Matter Model with Two Real Scalars*, *JCAP* **1503** (2015) 011, [1312.7488].
- [71] I. Brivio, M. B. Gavela, L. Merlo, K. Mimasu, J. M. No, R. del Rey et al., *Non-linear Higgs portal to Dark Matter*, *JHEP* **04** (2016) 141, [1511.01099].
- [72] N. Fonseca, R. Zukanovich Funchal, A. Lessa and L. Lopez-Honorez, *Dark Matter Constraints on Composite Higgs Models*, *JHEP* **06** (2015) 154, [1501.05957].
- [73] T. Cohen, J. Kearney, A. Pierce and D. Tucker-Smith, *Singlet-Doublet Dark Matter*, *Phys. Rev.* **D85** (2012) 075003, [1109.2604].
- [74] C. Cheung and D. Sanford, *Simplified Models of Mixed Dark Matter*, *JCAP* **1402** (2014) 011, [1311.5896].
- [75] F. Giacchino, A. Ibarra, L. Lopez Honorez, M. H. G. Tytgat and S. Wild, *Signatures from Scalar Dark Matter with a Vector-like Quark Mediator*, *JCAP* **1602** (2016) 002, [1511.04452].
- [76] S. Baek, P. Ko and P. Wu, *Top-philic Scalar Dark Matter with a Vector-like Fermionic Top Partner*, *JHEP* **10** (2016) 117, [1606.00072].
- [77] G. Belanger and J.-C. Park, *Assisted freeze-out*, *JCAP* **1203** (2012) 038, [1112.4491].
- [78] A. Biswas, D. Majumdar, A. Sil and P. Bhattacharjee, *Two Component Dark Matter : A Possible Explanation of 130 GeV γ - Ray Line from the Galactic Centre*, *JCAP* **1312** (2013) 049, [1301.3668].
- [79] S. Bhattacharya, P. Poulose and P. Ghosh, *Multipartite Interacting Scalar Dark Matter in the light of updated LUX data*, 1607.08461.
- [80] A. Drozd, B. Grzadkowski and J. Wudka, *Multi-Scalar-Singlet Extension of the Standard Model - the Case for Dark Matter and an Invisible Higgs Boson*, *JHEP* **04** (2012) 006, [1112.2582].
- [81] I. M. Hierro, S. F. King and S. Rigolin, *Higgs portal dark matter and neutrino mass and mixing with a doubly charged scalar*, 1609.02872.
- [82] K. Kawana, *Multiple Point Principle of the Standard Model with Scalar Singlet Dark Matter and Right Handed Neutrinos*, *PTEP* **2015** (2015) 023B04, [1411.2097].
- [83] M. Escudero, N. Rius and V. Sanz, *Sterile neutrino portal to Dark Matter I: The $U(1)_{B-L}$ case*, 1606.01258.

- [84] M. Escudero, N. Rius and V. Sanz, *Sterile Neutrino portal to Dark Matter II: Exact Dark symmetry*, 1607.02373.
- [85] S. Bhattacharya, S. Jana and S. Nandi, *Neutrino Masses and Scalar Singlet Dark Matter*, 1609.03274.
- [86] O. Fischer and J. J. van der Bij, *Multi-singlet and singlet-triplet scalar dark matter*, *Mod. Phys. Lett.* **A26** (2011) 2039–2049.
- [87] G. Arcadi, C. Gross, O. Lebedev, S. Pokorski and T. Toma, *Evading Direct Dark Matter Detection in Higgs Portal Models*, 1611.09675.
- [88] K. Ghorbani and H. Ghorbani, *Scalar split WIMPs in future direct detection experiments*, *Phys. Rev.* **D93** (2016) 055012, [1501.00206].
- [89] K. Kannike, *Vacuum Stability of a General Scalar Potential of a Few Fields*, *Eur. Phys. J.* **C76** (2016) 324, [1603.02680].
- [90] ATLAS collaboration, G. Aad et al., *Search for invisible decays of a Higgs boson using vector-boson fusion in pp collisions at $\sqrt{s} = 8$ TeV with the ATLAS detector*, *JHEP* **01** (2016) 172, [1508.07869].
- [91] ATLAS, CMS collaboration, G. Aad et al., *Measurements of the Higgs boson production and decay rates and constraints on its couplings from a combined ATLAS and CMS analysis of the LHC pp collision data at $\sqrt{s} = 7$ and 8 TeV*, *JHEP* **08** (2016) 045, [1606.02266].
- [92] CMS collaboration, C. Collaboration, *Searches for invisible Higgs boson decays with the CMS detector.*, CMS-PAS-HIG-16-016.
- [93] A. Belyaev, N. D. Christensen and A. Pukhov, *CalcHEP 3.4 for collider physics within and beyond the Standard Model*, *Comput. Phys. Commun.* **184** (2013) 1729–1769, [1207.6082].
- [94] J. M. Alarcon, J. Martin Camalich and J. A. Oller, *The chiral representation of the πN scattering amplitude and the pion-nucleon sigma term*, *Phys. Rev.* **D85** (2012) 051503, [1110.3797].
- [95] J. M. Alarcon, L. S. Geng, J. Martin Camalich and J. A. Oller, *The strangeness content of the nucleon from effective field theory and phenomenology*, *Phys. Lett.* **B730** (2014) 342–346, [1209.2870].
- [96] L. Alvarez-Ruso, T. Ledwig, J. Martin Camalich and M. J. Vicente-Vacas, *Nucleon mass and pion-nucleon sigma term from a chiral analysis of lattice QCD data*, *Phys. Rev.* **D88** (2013) 054507, [1304.0483].

- [97] R. D. Young, *Strange quark content of the nucleon and dark matter searches*, *PoS LATTICE2012* (2012) 014, [1301.1765].
- [98] ETM collaboration, A. Abdel-Rehim, C. Alexandrou, M. Constantinou, K. Hadjiyiannakou, K. Jansen, C. Kallidonis et al., *Direct Evaluation of the Quark Content of Nucleons from Lattice QCD at the Physical Point*, *Phys. Rev. Lett.* **116** (2016) 252001, [1601.01624].
- [99] M. Duerr, F. Kahlhoefer, K. Schmidt-Hoberg, T. Schwetz and S. Vogl, *How to save the WIMP: global analysis of a dark matter model with two s-channel mediators*, *JHEP* **09** (2016) 042, [1606.07609].
- [100] SUPERCDMS collaboration, R. Agnese et al., *Search for Low-Mass Weakly Interacting Massive Particles with SuperCDMS*, *Phys. Rev. Lett.* **112** (2014) 241302, [1402.7137].
- [101] CRESST collaboration, G. Angloher et al., *Results on light dark matter particles with a low-threshold CRESST-II detector*, *Eur. Phys. J.* **C76** (2016) 25, [1509.01515].
- [102] G. Belanger, F. Boudjema, A. Pukhov and A. Semenov, *micrOMEGAs3: A program for calculating dark matter observables*, *Comput. Phys. Commun.* **185** (2014) 960–985, [1305.0237].
- [103] G. Bélanger, F. Boudjema, A. Pukhov and A. Semenov, *micrOMEGAs4.1: two dark matter candidates*, *Comput. Phys. Commun.* **192** (2015) 322–329, [1407.6129].
- [104] FERMI-LAT, MAGIC collaboration, M. L. Ahnen et al., *Limits to dark matter annihilation cross-section from a combined analysis of MAGIC and Fermi-LAT observations of dwarf satellite galaxies*, *JCAP* **1602** (2016) 039, [1601.06590].
- [105] FERMI-LAT collaboration, M. Ackermann et al., *Updated search for spectral lines from Galactic dark matter interactions with pass 8 data from the Fermi Large Area Telescope*, *Phys. Rev.* **D91** (2015) 122002, [1506.00013].
- [106] J. Einasto, *On constructing models of stellar systems. V. The binomial model*, *Publications of the Tartuskoj Astrofizica Observatory* **36** (1968) 414.
- [107] J. F. Navarro, E. Hayashi, C. Power, A. Jenkins, C. S. Frenk, S. D. M. White et al., *The Inner structure of Lambda-CDM halos 3: Universality and asymptotic slopes*, *Mon. Not. Roy. Astron. Soc.* **349** (2004) 1039, [astro-ph/0311231].
- [108] J. F. Navarro, C. S. Frenk and S. D. M. White, *The Structure of cold dark matter halos*, *Astrophys. J.* **462** (1996) 563–575, [astro-ph/9508025].

- [109] J. F. Navarro, C. S. Frenk and S. D. M. White, *A Universal density profile from hierarchical clustering*, *Astrophys. J.* **490** (1997) 493–508, [[astro-ph/9611107](#)].
- [110] D. Feldman, Z. Liu and P. Nath, *PAMELA Positron Excess as a Signal from the Hidden Sector*, *Phys. Rev.* **D79** (2009) 063509, [[0810.5762](#)].
- [111] M. Ibe, H. Murayama and T. T. Yanagida, *Breit-Wigner Enhancement of Dark Matter Annihilation*, *Phys. Rev.* **D79** (2009) 095009, [[0812.0072](#)].
- [112] W.-L. Guo and Y.-L. Wu, *Enhancement of Dark Matter Annihilation via Breit-Wigner Resonance*, *Phys. Rev.* **D79** (2009) 055012, [[0901.1450](#)].
- [113] D. Albornoz Vasquez, G. Belanger and C. Boehm, *Astrophysical limits on light NMSSM neutralinos*, *Phys. Rev.* **D84** (2011) 095008, [[1107.1614](#)].
- [114] A. Chatterjee, D. Das, B. Mukhopadhyaya and S. K. Rai, *Right Sneutrino Dark Matter and a Monochromatic Photon Line*, *JCAP* **1407** (2014) 023, [[1401.2527](#)].
- [115] M. E. Peskin and D. V. Schroeder, *An Introduction to quantum field theory*. Addison-Wesley (1995) 842 p, 1995.